Energy Conversion and Management 77 (2014) 458–468

Contents lists available at ScienceDirect

Energy Conversion and Management

journal homepage: www.elsevier.com/locate/enconman

Thermoelectric-hydraulic performance of a multistage integrated thermoelectric power generator

B.V.K. Reddy, Matthew Barry, John Li, Minking K. Chyu *

Department of Mechanical Engineering and Materials Science, University of Pittsburgh, Pittsburgh, PA 15261, USA

ARTICLE INFO

Article history:
Received 2 May 2013
Accepted 18 September 2013

Keywords:
Flow channel
Integrated
Numerical model
Performance
Thermoelectrics
Waste-heat recovery

ABSTRACT

A thermoelectric element made of *p*- and *n*-type semiconductor plates bonded onto a highly thermal and electrical conducting inter-connector material with an integrated flow channel can be treated as an integrated thermoelectric device (iTED). The performance of an iTED with multiple elements connected electrically in series and thermally in parallel has been investigated using numerical simulations. The top and bottom surfaces of the device are subjected to a constant cold temperature while the inter-connector channel walls are exposed to a hot fluid. The thermoelectric-hydraulic behavior of an iTED is analyzed in terms of heat input, power output, conversion efficiency, produced electric current, Ohmic and Seebeck voltages, and pressure drops for various hot fluid flow rates *Re* and inlet temperatures T_{in}, thermoelectric material sizes *d*, and number of modules *N*. For a single module iTED with fixed *d* and T_{in} values, the power output and efficiency are increased five- and twofold, respectively at *Re* = 500 when compared with the values of *Re* = 100. For given *Re* and *d* values, increasing T_{in} resulted in enhanced device performance. Furthermore, increasing *d* increased internal resistance and resulted in a decrease of heat input. The influence of *d* on power output is phenomenal; for a given set of geometric and thermal boundary conditions, there exists an optimum *d* where a maximum power output is achieved. The addition of modules *N* resulted in a significant improvement in power output and a reduction in produced electric current and efficiency. For instance, device with *N* = 5 showed more than a twofold increase in power output and nearly a 33% reduction in both efficiency and electric current when compared to *N* = 1 values.

1. Introduction

There is an ever-increasing amount of green-house gas and waste-heat released into the atmosphere from the fossil-fuel power generation plants, automobiles, and industrial heating or cooling systems in response to continual energy demands. Approximately two -thirds of the supplied energy into these systems is rejected as a waste-heat to the surroundings. There is an urgent need to explore novel, environmentally-friendly technologies that can replace or improve the performance of the existing systems. Solid-state thermoelectric devices are a viable technology for recovering waste-heat and convert it into electricity while mitigating the emission of green-house gases.

Thermoelectric devices (TEDs) are constructed by joining two different electrically and thermally conductive materials at a junction. Using the Seebeck effect, TEDs work as electric power generators when the two material junctions are exposed to a temperature differential. Similarly, TEDs act as a refrigerators via the Peltier effect when an electric current is applied across the terminals, creating a temperature differential at the material junction [1]. However, the current thermoelectric materials with a figure of merit ≈1.5 achieve thermal conversion efficiencies of 5–15% and coefficients of performance (COP) of 0.5–1. Due to their scalable, reliable, stable, compact and noise free operation, TEDs are suitable in novel applications such as waste-heat recovery from exhaust streams and other low-grade heat sources, electric power generation for remote radio and satellite stations, pocket electronics, bio-thermal batteries to power pacemakers, localized cooling in electronic components and space cooling in automobile seats.

The efficiency of TEDs has been increased via the methods of nano-structuring and fabrication [2–4], novel designs [5–10] and use of new bulk materials [1]. Caillat et al. [5] developed a segmented TED using novel *p*- and *n*-type materials, and achieved a conversion efficiency of 15%. El-Genk et al. [6] reported peak efficiencies of 16.69% and 7.4% respectively for skutterudite and SiGe segmented TEDs. Further, Punnachaiya et al. [7] studied cascaded TEDs and showed a low conversion efficiency of 0.47% with T_h = 96 °C and temperature differential (T_h–T_c) of 25 °C. Liang et al. [8] investigated the performance of a multistage TED and

* Corresponding author. Tel.: +1 412 624 9720; fax: +1 412 624 4846.
E-mail addresses: bvkreddy680@gmail.com (B.V.K. Reddy), mmb49@pitt.edu (M. Barry), johnli407@yahoo.com (J. Li), mkchyu@pitt.edu (M.K. Chyu).

0196-8904/$ - see front matter © 2013 Elsevier Ltd. All rights reserved.
http://dx.doi.org/10.1016/j.enconman.2013.09.040

Nomenclature

A	cross-sectional area, mm^2
c_p	specific heat of fluid, $Jkg^{-1}\,K^{-1}$
d	size of semiconductor material, mm
D	depth of the thermoelectric leg, mm
D_h	hydraulic diameter of main flow channel $\left(\frac{4(H-2d)\times D}{2(H-2d+D)}\right)$, mm
H	height of the leg, mm
I	electric current, A
J	electric current density $A\,m^{-2}$
$\mathbf{J}$	current density vector
k	thermal conductivity, $Wm^{-1}\,K^{-1}$
L	distance between the legs, mm
N	number of thermoelectric modules
P	pressure, $N\,m^{-2}$
P_0	power output (I^2R_L), W
Q	heat transfer, W
R	electrical resistance, Ω
Re	Reynolds number ($\rho UD_h/\mu$)
t	connector thickness, mm
T	temperature, K
U	inlet velocity, $m\,s^{-1}$
$\mathbf{v}$	velocity vector
V	voltage, V
u, v, w	velocities in x, y, z directions, $m\,s^{-1}$
W	width, mm
x, y, z	coordinates, mm

Greek symbols

α	Seebeck coefficient or thermopower, $V\,K^{-1}$
μ	dynamic viscosity, $N\,s\,m^{-2}$
ρ	electrical resistivity, Ω m
ρ_f	density of fluid, $kg\,m^{-3}$
η	thermoelectric conversion efficiency, dimensionless

Subscripts

c	cold wall/conductor
in	inlet
f	fluid
h	hot wall
i	internal/integrated
ic	inter-connector
L	load
n	n-type semiconductor
O	Ohmic potential
p	p-type semiconductor
S	Seebeck potential
ξ	direction normal to the surface

they demonstrated that the thermal contact resistance between the TED module and heat source or sink plays a substantial role in the power output. Recently, Crane et al. [9] built a full-scale cylindrical-shaped thermoelectric generator using segmented and high-power density elements and produced a power output of 608 W.

Using analytical solutions and experiments, Gou et al. [11] showed that expanding the heat sink surface area and enhancing the cold side heat transfer in proper ranges can have significant effects on TEDs performance when compared to increasing the waste-heat temperature and addition of modules in series. Further, Hasio et al. [12] investigated TED applied to waste-heat recovery from an automobile engine and showed that the TED performs better on the exhaust pipe than radiator. Even though electric and temperature fields in TEDs are multidimensional, most of the works in literature were conducted with one-dimensional analytical solutions for simplified cases. However, for accurate system design and optimization of TEDs, the three-dimensional (3D) numerical studies have been conducted in the articles [13–20,22]. Further, Karri et al. [21] investigated the performance of various modeling approaches for thermoelectric elements and their merits and demerits under given geometric and thermal boundary conditions.

Harris et al. [13] studied the influence of inert gas and insulating materials, and interface contact resistances on TED performance using finite volume numerical methods. Considering the convection and radiation effects, Ziolkowski et al. [14] studied the performance of TED in ANSYS software for various pellet aspect ratios and contact resistances. Gould et al. [22] simulated the TED configured for low power generation using TCAD package. In the articles [15,16], the authors used numerical simulations to study the optimum geometries of TEDs to achieve a maximum conversion efficiency. Furthermore, the researchers [17,19] proposed and implemented a 3D numerical model for thermoelectric generators in FLUENT UDS environment and their model accounts for all temperature-dependent properties of materials and non-linear fluid-thermal-electric multi-physics coupled effects. Recently, by coupling both temperature and electric potential fields Wang et al. [18,20] studied the steady and transient response of TEDs using 3D multi-physics models.

It is observed from literature that the conventional TED designs applied to waste-heat recovery induce large thermal resistance between the working fluid and the thermoelectric junctions via the heat exchanger, ceramic plate, and the interface materials, and also they require great amounts of semiconductor materials for module construction due to the demand of constant leg heights for fabrication ease. Keeping this in mind, the authors proposed an integrated thermoelectric device (iTED) [23,24] where the hot-side inter-connector is re-designed to incorporate an integrated heat exchanger. By doing so, this novel design reduces the thermal resistances attributed to the heat sinks and ceramic plates, which are present in convectional design. Further, by adjusting the height of the inter-connector heat exchanger, this design would help in using different semiconductor element heights for achieving maximum power output and efficiency while keeping the height of the module invariant. In essence, this design enhances reliability and performance of TED. In this study, using numerical methods the thermoelectric-hydraulic performance of such a iTED with multiple modules connected electrically in series and thermally parallel is investigated. The effects of heat exchanger hot fluid flow rates and inlet temperatures, thermoelectric element sizes, and the number of modules on the performance of an iTED applied to waste-heat recovery under steady state conditions (the performance variation with respect to the time is zero) are studied in detail.

2. Geometry, governing equations, and boundary conditions

The schematic of the three-dimensional single-stage integrated thermoelectric device (iTED) being investigated is shown in Fig. 1a. The device consists of two vertical legs connected electrically in series and thermally in parallel via connectors made of highly electrical conducting material. Each thermoelectric leg is constructed

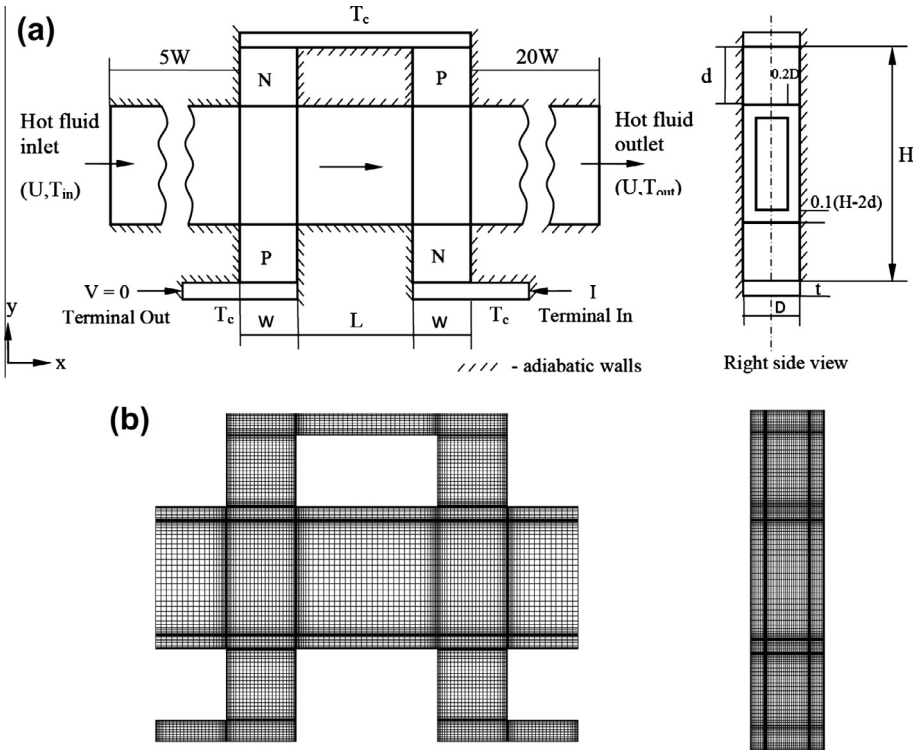

Fig. 1. Schematic of (a) single-stage integrated thermoelectric device and (b) mesh.

by inserting a copper inter-connector with an integrated flow channel acting as a heat exchanger between *n*- and *p*-type semiconductor slices. A square cross-section $W \times D$ and height H is considered for each leg and the legs are separated by a distance L as shown in Fig. 1a. The inter-connector channel of rectangular shape with size $0.6D \times 0.8(L-2d) \times W$ is taken for fluid flow. A hot fluid with constant temperature T_{in} and uniform velocity U enters the main flow channel of invariant cross-sectional area $D \times (L-2d)$ and passes through inter-connector channel and leaves at the exit of the fluid domain (Fig. 1a). The channel walls and the up and down stream side surfaces of inter-connector are solely responsible for the heat transfer from the hot fluid to the thermoelectric elements. The top surface of the upper connector and the lower surface of the bottom connectors are maintained at a constant cold temperature T_c. The remaining surfaces of the iTED and the main flow channel walls are kept adiabatic.

The iTED generates electrical power through a temperature differential $(T_h - T_c)$ present between the inter-connector channel walls and the cold surface via the Seebeck effect when it is connected to a load resistance R_L. The fluid flow and the heat transport in the fluid domain are governed by the conservation of mass, momentum, and energy equations while subjected to the following assumptions: the flow is steady, laminar and incompressible, and the thermophysical properties of fluid are kept constant. Thermoelectric materials are heterogeneous and isotropic. Furthermore, the current flow and the heat transport in thermoelectric materials are governed by the continuity of current density and the energy equations, respectively.

The set of partial differential equations governing the incompressible fluid flow and heat transport in the fluid domain and the thermoelectric phenomenon in the conductor and semiconductor materials under steady-state conditions are written as:

- Continuity equations:
  - Fluid region:

$$\nabla.\mathbf{v} = 0. \tag{1}$$

  - Conductor and semiconductor material [1]:

$$\nabla.\mathbf{J} = 0. \tag{2}$$

- Momentum equation:

$$\rho_f(\mathbf{v}.\nabla\mathbf{v}) = \nabla P + \mu\nabla^2\mathbf{v}. \tag{3}$$

- Energy equations:
  - Fluid region:

$$(\rho c_P)_f(\mathbf{v}.\nabla T) = \nabla.(k_f\nabla T). \tag{4}$$

  - Conductor material:

$$\nabla.(k\nabla T) + \rho\mathbf{J}^2 = 0. \tag{5}$$

  - Semiconductor material [1]:

$$\nabla.(k\nabla T) + \rho\mathbf{J}^2 - T\mathbf{J}.\left[(\nabla\alpha)_T + \left(\frac{\partial\alpha}{\partial T}\right)\nabla T\right] = 0. \tag{6}$$

The second and third terms in the left hand side of Eq. (6) represent the Joule heating and Peltier and Thomson effects, respectively. The Thomson effect as compared to Joule heating and Peltier effect does not contribute significantly to the performance of thermoelectric material. However, it has been included in the analysis for the completeness.

Using the non-Ohmic current–voltage [25] relation, the total electric potential is calculated as

$$\nabla V = \nabla V_O + \nabla V_S = -\rho\mathbf{J} - \alpha\nabla T \tag{7}$$

In Eq. (7), the first term on the right hand side is the electrostatic potential distribution due to current flowing in the material and the second term comprises the Seebeck electric potential distribution via the temperature differential created in the thermoelectric material.

With respect to the geometry shown in Fig. 1a, the associated thermal and electrical boundary conditions for solving Eqs. (1)–(7) are:

At the '*in*' terminal:

$$J = \frac{I}{A_\xi} = \frac{V_{oc}}{A_\xi (R_i + R_L)} \quad \text{and} \quad \frac{\partial T}{\partial \xi} = 0 \tag{8}$$

where V_{oc} is the Seebeck voltage, the total built-in open circuit voltage in the iTED at no-load condition. In Eq. (8), ξ, A and R_L represent the direction normal to the surface, the cross-sectional area and the external load resistance, respectively.

The V_{oc} is calculated as the summation of the Seebeck potentials at the interfaces of the semiconductor and conductor materials and it is written as:

$$V_{oc} = \sum_{j=n,p} \sum_{i=1}^{2N} \frac{1}{A_{ji}} \int_{A_{ji}} |\alpha_{ji}| \frac{dT}{d\xi} dA \tag{9}$$

The Seebeck potentials are evaluated with reference to the hot surface temperatures at the interface of the semiconductor and inter-connector materials. In Eq. (9), A is the interface surface area at the junction between the thermoelectric material and the connector.

Further, in Eq. (8), R_i is the total internal resistance which is the summation of the electrical resistivities of the n- and p-type slices, the connectors and the inter-connector materials and it is evaluated as:

$$R_i = \sum_{j=n,p,c,ic} \sum_{i=1}^{2N} \frac{H_{ji}}{A_{ji}} \left[\frac{1}{V_{ji}} \int_{V_{ji}} \rho_{ji} dv \right] \tag{10}$$

where H, A and V are the height, cross-sectional area, and volume of the electrical material, respectively. In Eqs. (9) and (10), j is the material type (n, p, connector and inter-connector), i is the number of vertical legs and N is the number of modules, i.e. each module has two vertical legs as shown in Fig. 1a.

At the '*out*' terminal:

$$V = 0 \quad \text{and} \quad \frac{\partial T}{\partial \xi} = 0 \tag{11}$$

At the top surface of the upper connector and the bottom surfaces of the lower connectors:

$$T = T_c \quad \text{and} \quad \frac{\partial V}{\partial \xi} = 0 \tag{12}$$

At all other surfaces exposed to surroundings:

$$\frac{\partial T}{\partial \xi} = 0 \quad \text{and} \quad \frac{\partial V}{\partial \xi} = 0 (\text{iTED}); \quad \frac{\partial T}{\partial \xi} = 0 \text{ main flow channel} \tag{13}$$

At the fluid flow inlet:

$$x = 0: \quad u = U, v = w = 0 \quad \text{and} \quad T = T_{in} \tag{14}$$

At the fluid flow outlet:

$$x = 5W + N(2W + L) + 20W: \quad \frac{\partial u}{\partial \xi} = \frac{\partial T}{\partial \xi} = v = w = 0 \tag{15}$$

At the interface between the semiconductor and connector or inter-connector materials, the continuity of temperature, current density and the heat flux conditions are imposed and are written as:

$$T_{c,ic} = T_{n,p}, \quad \mathbf{J}_{c,ic} = \mathbf{J}_{n,p} \quad \text{and} \quad -\frac{dT_{c,ic}}{d\xi} = -\frac{k_{n,p}}{k_{c,ic}} \frac{dT_{n,p}}{d\xi} \tag{16}$$

The power output P_0 from the iTED for a given load resistance R_L and the heat input Q_h into the iTED are evaluated as:

$$P_0 = I^2 R_L \quad \textit{and} \quad Q_h = -\sum_{i=1}^{2N} \frac{1}{As_i} \int_{As_i} k_f \frac{\partial T}{\partial \xi} dAs_i \tag{17}$$

where As is the surface area of inter-connector walls exposed to hot fluid.

The thermoelectric conversion efficiency of an iTED is calculated as

$$\eta = \frac{P_0}{Q_h}. \tag{18}$$

3. Numerical solution procedure, grid independence study, and validation

The numerical simulations are performed using the finite volume formulation of Eqs. (1)–(6) and the constitutive relation (7) along with associated boundary conditions Eq. (8) and Eqs. (11)–(15) in the FLUENT-UDS (User Defined Scalar) environment. The motivation for implementing the present numerical code in FLUENT is because this package has already well-defined fluid and heat transfer models, hence it allows the detailed investigation of fluid-thermo-electrical coupled phenomenon in iTEDs. The pressure–velocity coupling is handled using SIMPLE algorithm [26]. The spatial descretisation of convective and diffusive terms is done with a power law scheme and the pressure term is handled with a standard scheme. The geometric models and mesh are generated in Gambit 2.4. The Seebeck potential and Ohmic electric potential distributions (Eq. (7)) and continuity of current density (Eq. (2)) are calculated using UDS fields. The Ohmic heating, Peltier and Thomson effects are modeled as source terms in the energy equation (Eq. (6)). The electric current is evaluated based on the Seebeck voltage (Eq. (9)) produced at a given load resistance R_L, as given in Eq. (10). A further detailed description on numerical implementation of TED governing equations in the FLUENT-UDS has been given in the articles [17,19].

The convergence criteria (the difference between consecutive iterations over a domain) for mass and momentum, energy, current density, Seebeck and Ohmic electric potentials are set as 10^{-5}, 10^{-15}, 10^{-10}, 10^{-10}, and 10^{-10}, respectively. After performing a grid independence study, suitable grid sizes were chosen for further numerical simulations on iTEDs. Grid sizes with 1,574,424, 2,303,208, 2,906,712, 3,760,776 and 4,489,560 cells are used for one-to-five modules iTEDs, respectively, to generate results. For

Table 1
Grid independence study for single-stage integrated thermoelectric device (grid size in bold face is chosen for further simulations) [Re = 500, T_{in} = 550 K, T_c = 300 K, d = 5 mm and $R_L = 6.5 \times 10^{-3}$ Ω].

Cells	P_0 W	% of error in P_0	Q_h W	% of error in Q_h	η %	% of error in η
406,572	0.0929		2.8211		3.2932	
713,880	0.0949	2.1072	2.7833	1.3577	3.4098	3.4185
1,574,424	0.0959	1.0828	2.7652	0.6556	3.4697	1.7271
2,392,952	0.0955	0.4244	2.7594	0.2074	3.4622	0.2166

Table 2
Dimensions of an integrated thermoelectric device.

H (mm)	D (mm)	W (mm)	t (mm)	L (mm)	d (mm)
20	5	5	1.5	10	0.25, 1, 3, 5, 7

brevity, the grid independence test conducted on a single-stage iTED (as shown in Fig. 1a) is depicted in Table 1. Further, the orthogonal, nonuniform grid used for a single-stage iTED along the sectional plane (as shown in side view of Fig. 1a) is also shown in Fig. 1b. The implemented thermoelectric model has been validated with published results and are given in our previous works [19,23].

4. Results and discussion

Using the implemented fluid-thermo-electric coupled field numerical code in the FLUENT UDS environment as presented in the previous section, the thermoelectric performance of an integrated thermoelectric device (iTED) applied to waste-heat recovery has been investigated. In this study, the effects of various parameters: hot fluid inlet temperatures $350 \leqslant T_{in}(K) \leqslant 550$, semiconductor ($n$- and p-type) element sizes $0.25 \leqslant d(\text{mm}) \leqslant 7$ and the number of modules $1 \leqslant N \leqslant 5$ on the performance of an iTED expressed in terms of power output P_0, heat input Q_h, thermal conversion efficiency η, pressure drop $\Delta P/L$, produced electric current I and the Ohmic and Seebeck voltages V have been investigated for

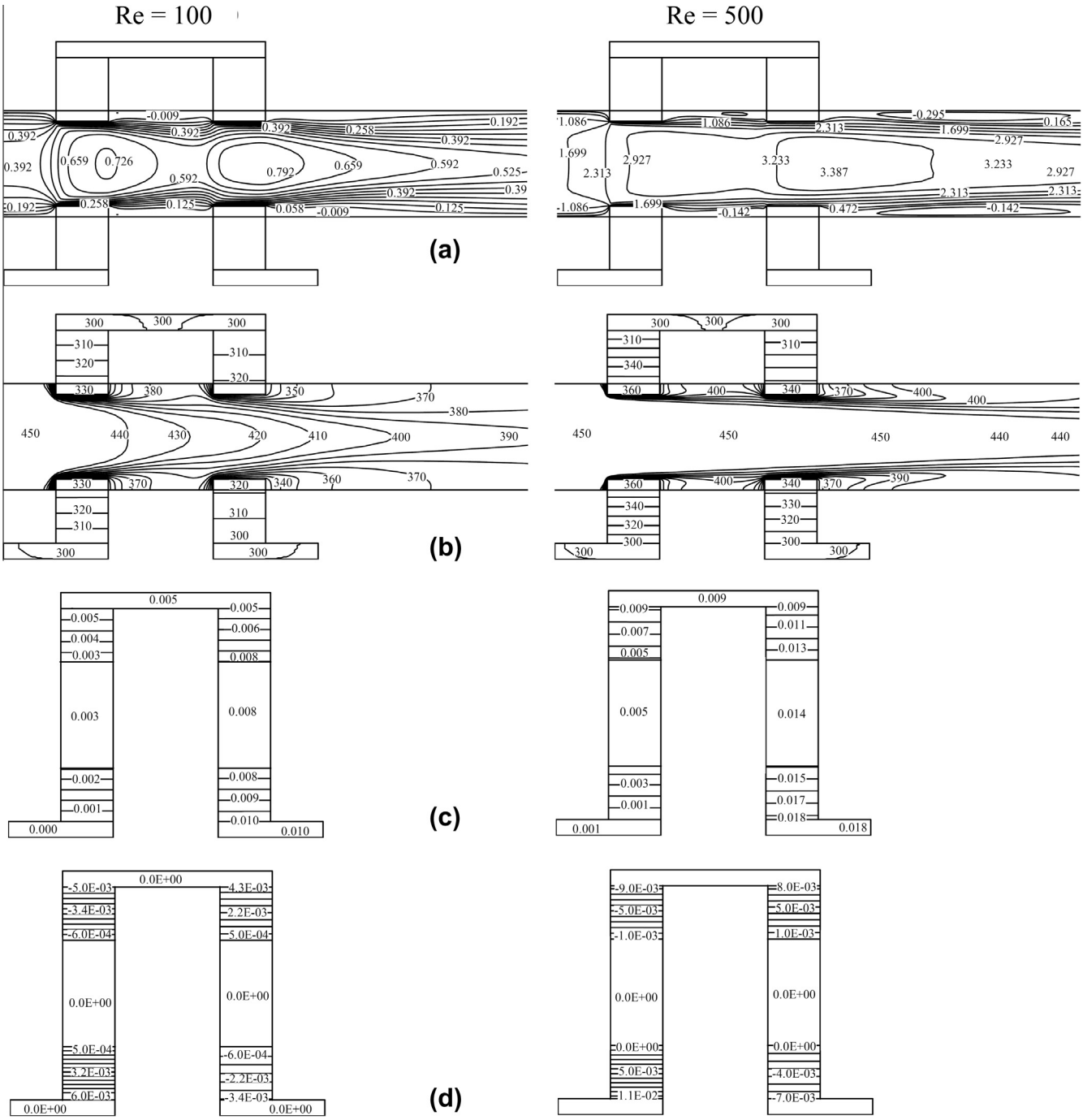

Fig. 2. Effects of *Re* on (a) *x*-velocity, (b) temperature contours, (c) Ohmic and (d) Seebeck voltage distributions [at T_{in} = 450 K, T_c = 300 K, d = 5 mm and $R_L = R_i$].

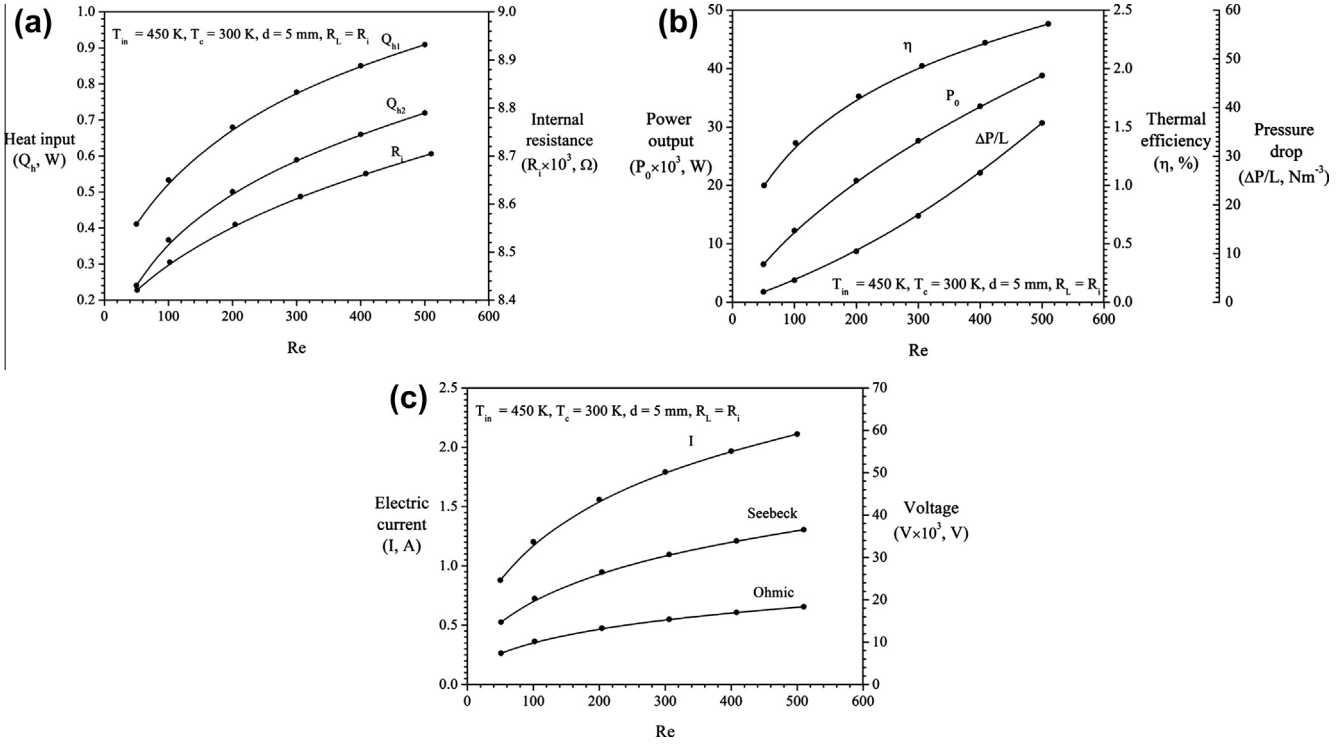

Fig. 3. Effects of *Re* on (a) heat input and load resistance, (b) power output and thermal efficiency and (c) electric current and voltages.

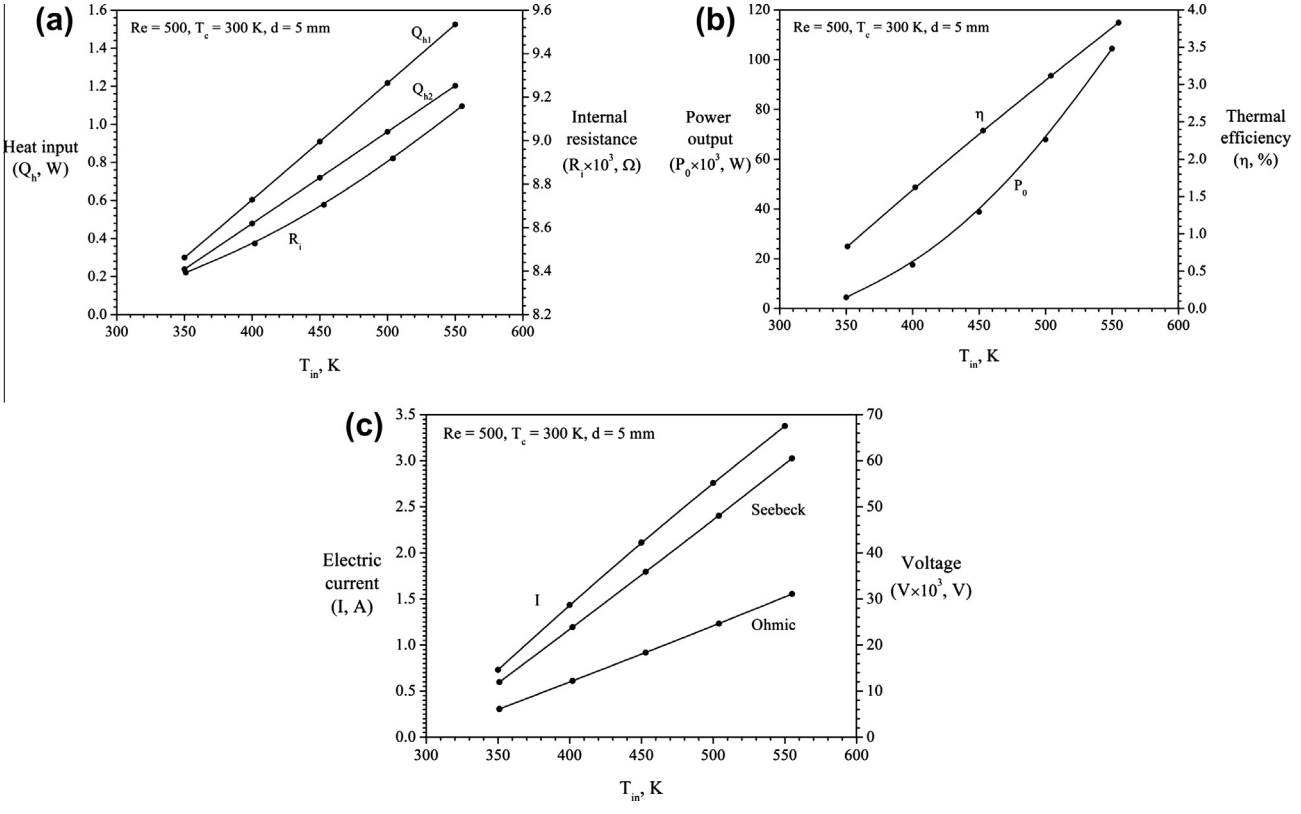

Fig. 4. Influence of hot fluid inlet temperature T_{in} on (a) heat input and load resistance, (b) power output and thermal efficiency and (c) electric current and voltages.

various fluid flow configurations $50 \leqslant Re \leqslant 500$. The dimensions of an iTED used in the numerical simulations (as shown in Fig. 1a) are given in Table 2.

The thermoelectric materials are treated as bulk bismuth–telluride–antimony–selenium: *n*-type ($75\%Bi_2Te_3 25\%Bi_2Se_3$) and *p*-type ($25\%Bi_2Te_3 75\%Sb_2Te_3$ (1.75% excess Se)). Copper is used for the

conductor and air is the hot fluid. Further, the thermo-electrical properties of the semiconductor (Seebeck coefficient α, electrical resistivity ρ and thermal conductivity k) and conductor (ρ and k) materials are temperature-dependent (as reported in article [23], in Table 1) while the thermo-physical properties of air are kept constant. For the numerical simulations, the maximum power output P_0 from the iTED is achieved when the load resistance R_L equals the total internal resistance R_i (Eq. (10)), and thus all cases use this relation.

For a single-stage iTED, the contours of x-velocity and isotherms at section z = 2.5 mm and Ohmic and Seebeck voltage distributions at z = 0.5 mm are shown in Fig. 2 for Re values of 100 and 500. Here, T_{in} = 450 K and d = 5 mm are kept constant. For clarity, as displayed in Fig. 2a and b, an upstream length W and a downstream length 5 W are chosen for depicting x-velocity and temperature distributions. From Fig. 2b, it is seen that an increase in temperature gradients in the fluid region at the inter-connector channel walls when Re is increased from 100 to 500. This increase in temperature gradients helps in enhancement of convective heat transfer and thus eventually results in a reduction of the total thermal resistance of the iTED. Furthermore, the recirculation zones formed in the up and down streams of iTED and in between the legs have minimal effect on device performance. However, the strength of the recirculation increases with an increase in Re values, as seen in Fig. 2a.

The increase in temperature differential T_h–T_c (between the inter-connector channel wall and the cold end surface) via increasing Re generates higher Seebeck voltages in the thermoelectric elements, as shown in Fig. 2d. In each element, the Seebeck voltage drop is calculated with respect to the connector (copper) material value; however, the Seebeck coefficient of copper is negligible compared to the semiconductor value. From Fig. 2d, at given a Re, it is noticed that due to presence of a larger T_h–T_c value in the left leg, the built-in Seebeck voltage is higher compared to the right leg value. On the other hand, as shown in Fig. 2c, as Re increased from 100 to 500, the Ohmic voltage drop increased from 0.017 to 0.031 V. Further, the Ohmic voltage drop in the copper material is negligible due to its lower electrical resistivity value (approximately three orders of magnitude smaller than semiconductor material value).

The effects of several flow configurations Re on iTED performance parameters Q_h, P_0 and η, and electrical characteristics I and V are shown in Fig. 3. The change in total internal resistance R_i and the pressure drop $\Delta P/L$ with Re are also depicted in Fig. 3a and b, respectively. Fig. 3a represents the heat transferred, as given by Q_{h1} and Q_{h2}, to the left and right legs of a single-stage iTED

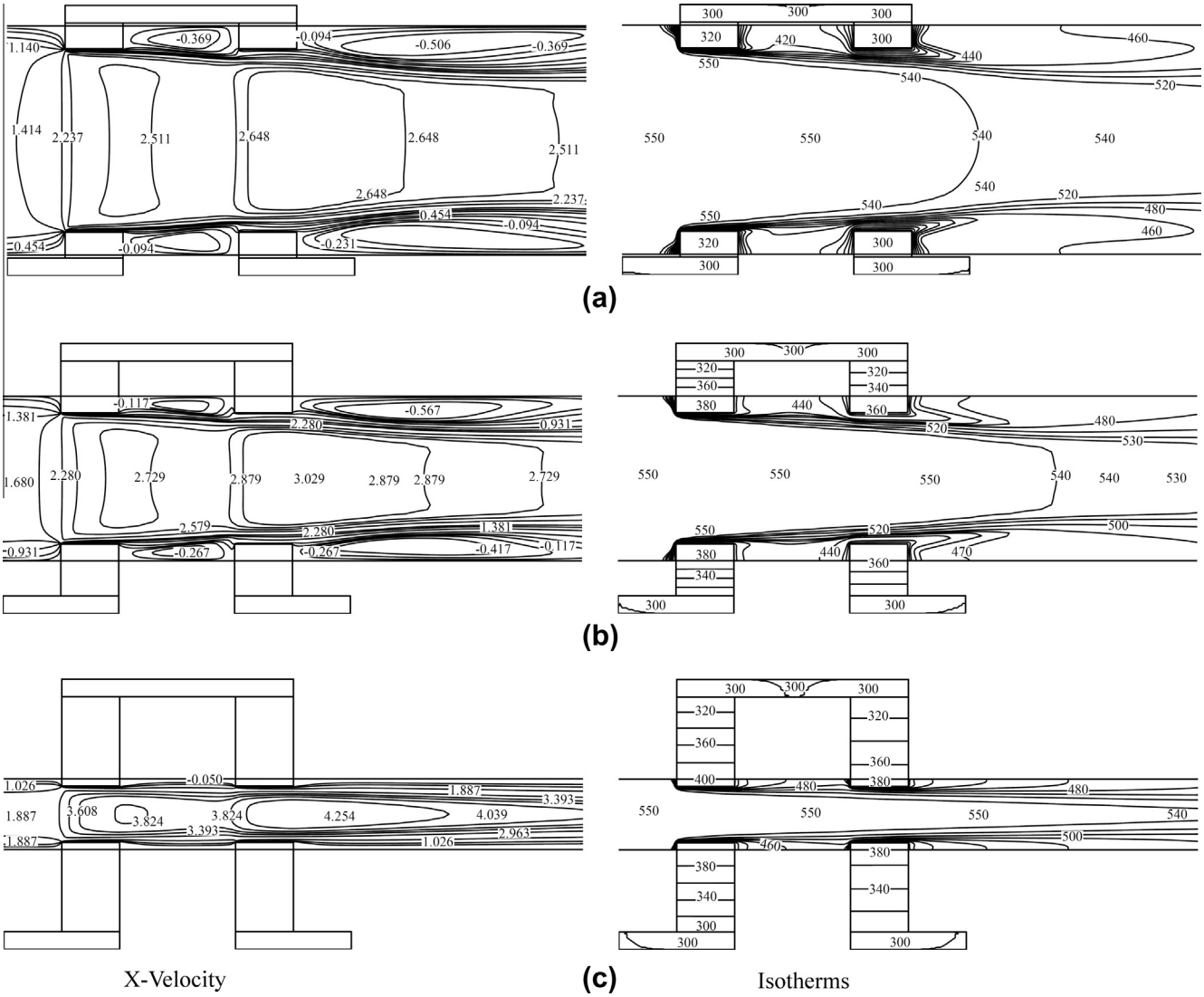

Fig. 5. The variation of x-velocity and temperature contours for different thermoelectric element heights d (mm) (a) 0.25 (b) 3 and (c) 7 of a single-stage thermoelectric device [at Re = 500, T_{in} = 550 K, T_c = 300 K and $R_L = R_i$].

module, respectively. For a given T_{in} = 450 K, an increase in *Re* shows an enhancement in Q_h and resulted in higher T_h–T_c values. The increase in T_h–T_c is due to the reduction of developing thermal boundary layer thickness over inter-connector channel walls as *Re* increases (as shown in Fig. 2b). As discussed earlier, the higher T_h–T_c values result in larger built-in Seebeck voltages which in turn results in a greater P_0 (as seen in Fig. 3b). At *Re* = 500, P_0 and η increase five- and twofold, respectively, as compared to the values at *Re* = 100. The produced current *I* and voltages *V* have shown similar trends with *Re*. From Fig. 3c, it is noticed that at a given *Re* value, the Ohmic voltage drop is higher than the Seebeck voltage drop value. Furthermore, the flow rate has a minimal effect on R_i predictions and merely a 3.3% variation is observed in R_i for the flow rate range of $50 \leqslant Re \leqslant 500$. This change merely is due to the variation in electrical resistivity value with temperature (Eq. (10)). As seen in Fig. 3b, the $\Delta P/L$ increases as *Re* is increases and shows a nonlinear behavior. The reason for this behavior is due to the cumulative effect of developing flow in the integrated flow channels and the formation of the recirculation zones in the main flow channel (as shown in Fig. 2a).

For a given $R_L = R_i$ condition, the variation in both thermal and electrical characteristics of a single-stage iTED module with hot fluid inlet temperatures T_{in} are shown in Fig. 4a–c. An increase in

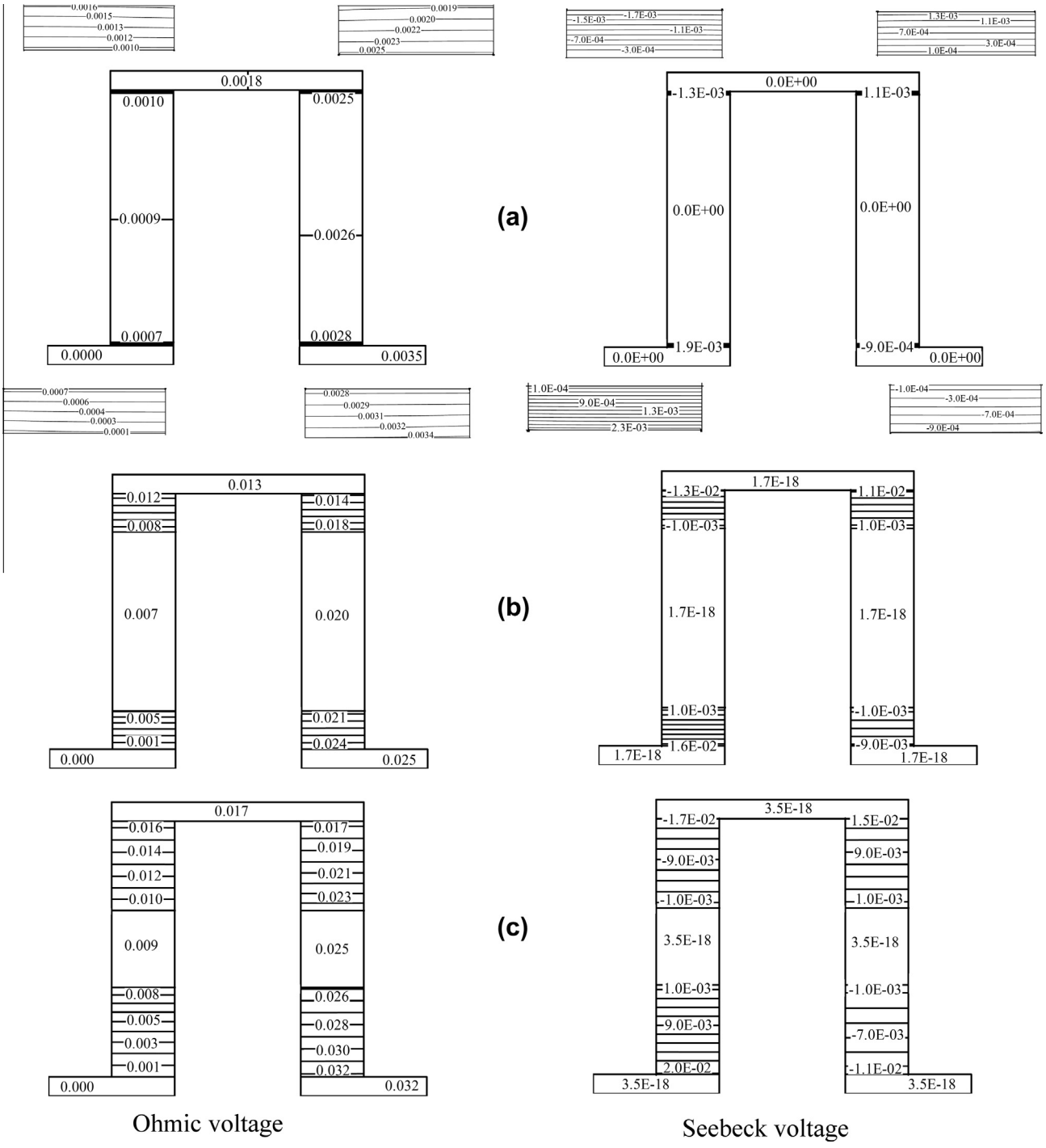

Fig. 6. The variation of Ohmic and Seebeck voltage distributions for different thermoelectric element heights *d* (mm) (a) 0.25 (b) 3 and (c) 7 of a single-stage thermoelectric device [at *Re* = 500, T_{in} = 550 K, T_c = 300 K and $R_L = R_i$].

T_{in} results in an enhancement in Q_h, P_0, η, I and V values. Further, a linear behavior in V–I (Eqs. (8)), Q_h (Eq. (17)) and η (Eq. (18)) values and a nonlinear trend in P_0 (Eq. (17)) and R_i (Eq. (10)) with T_{in} are observed. The reason for this nonlinear trend in R_i is due to the behavior of temperature-dependent electrical resistivity. Moreover, the increment in R_i with an increase in T_{in} is marginal and exhibited a 9.2% variation within the temperature range $350 \leqslant T_{in}(\mathrm{K}) \leqslant 550$ (as seen in Fig.4a).

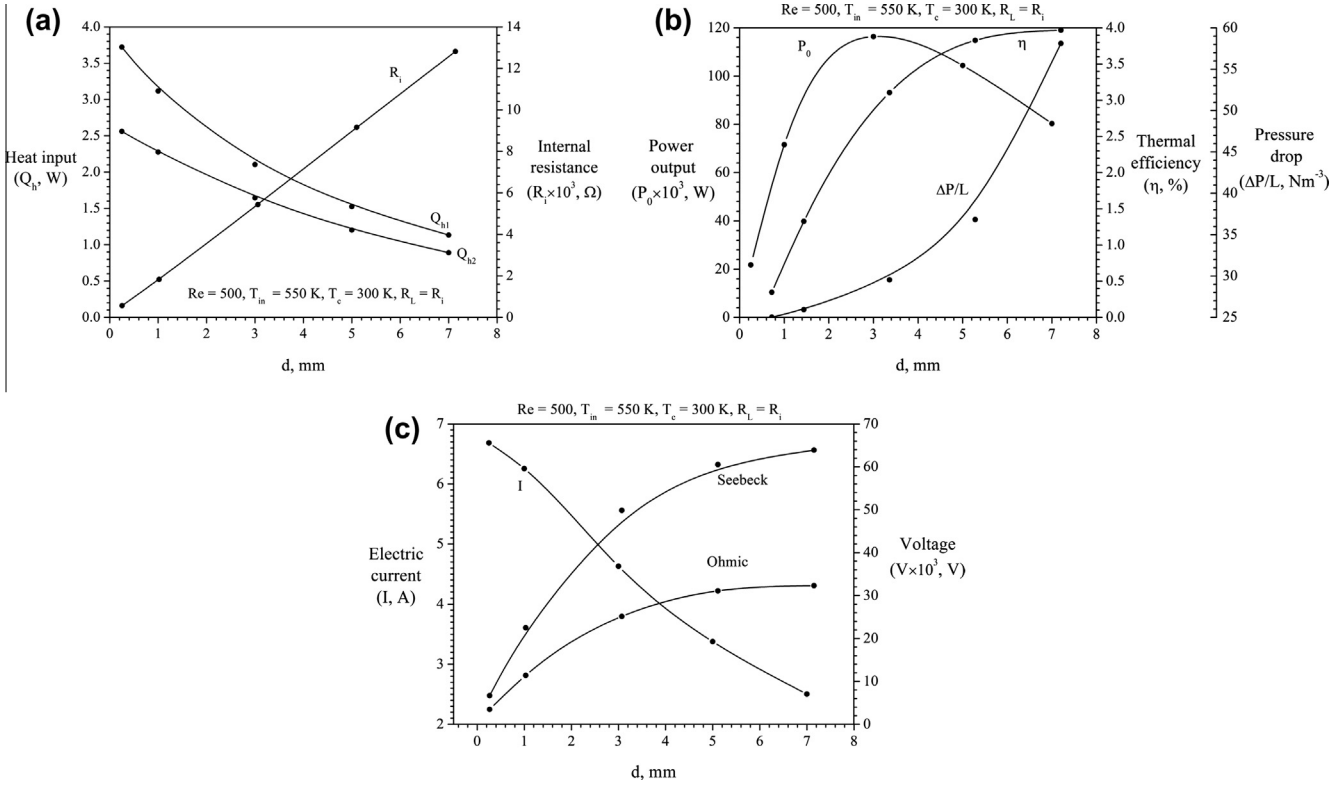

Fig. 7. The response of (a) heat input and load resistance, (b) power output and thermal efficiency and (c) electric current and voltages for different thermoelectric element heights d.

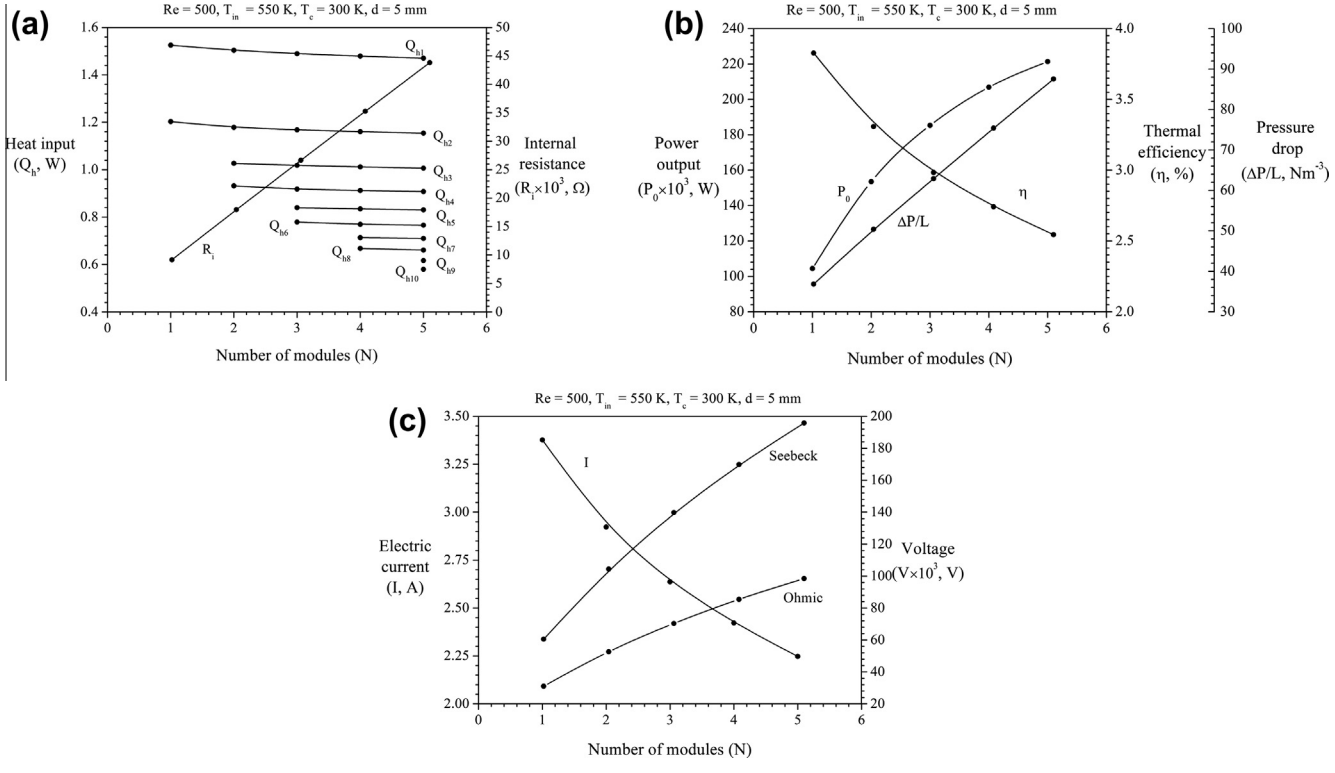

Fig. 8. The influence of number of modules N on (a) heat input and load resistance, (b) power output and thermal efficiency and (c) electric current and voltages.

Figs. 5 and 6 show the contours of x-velocity and temperatures at section $z = 2.5$ mm and the Ohmic and Seebeck potential distributions at $z = 0.5$ mm, respectively for three sizes of semiconductor elements d. Here, both the n- and p-type semiconductor elements are kept equal in size and also the height of the module is maintained constant. Hence, the modification in d effects inter-connector channel dimension $(H - 2d) \times W \times D$ as shown in Fig. 1a. For fixed $T_{in} = 550$ K and $Re = 500$, where Re is defined based on hydraulic diameter of the main flow channel $(H - 2d) \times D$, as d increases, both averaged velocity of fluid in the inter-connector channel and total thermal resistance of legs increase and hence, an increase in the inter-connector channel wall temperature is noticed. Further, the gain in T_h–T_c with an increase in d helps to enhance the total built-in Seebeck potential in the thermoelectric materials and also to achieve higher Ohmic voltage drop values (as shown in Fig. 6). It is noticed that an increase in d changes the developing flow behavior in the inter-connector channel, and thus the temperature distribution in the fluid and solid regions appears accordingly. The strength of recirculation in between the legs and the reattachment length in the downstream decrease with an increase in d value.

The response of iTED's thermoelectric–hydraulic characteristics for various thermoelectric material sizes d are presented in Fig. 7. As seen in Fig. 7a, the increase in d results in a linearly proportional gain in R_i values. Further, this R_i has a phenomenal effect on iTED's performance. When Re and T_{in} are fixed, the Q_h decreases with an increase in d which is due to the increase in the thermal resistance of the legs. However, at a given d, the left leg extracts more heat compared to right leg of the iTED. From Fig. 7b, it is observed that there exists a maximum P_0 at an optimum d value for a given set of operating parameters. This behavior is due to the mutual interplay of the total electrical resistance and the thermal resistance values of an iTED. Here, the total thermal resistance includes the summation of resistances due to semiconductor elements, connectors, convective heat transfer at the inter-connector channel walls and the constant temperature at the cold surfaces. On the other hand, The η of the iTED increases exponentially with an increase in d. For a fixed Re, the effect of d on $\Delta P/L$ is marginal and it is due to the increment in inlet velocity and the reduction in hydraulic diameter with an increase in d value. The T_h–T_c value improves with an increase in d and thus reflects in the total Seebeck voltage potential predictions (Fig. 7c). As shown in Fig. 7c, the produced current I reduces and the Ohmic voltage potential increases with a rise in d values and these trends are due to the increment in R_i values.

The performance of a multi-stage iTED for a various number of modules $(1 \leqslant N \leqslant 5)$ connected electrically in series and thermally in parallel is shown in Fig. 8. For all other parameters kept invariant ($Re = 500$, $T_{in} = 550$ K, $T_c = 300$ K and $d = 5$ mm), the R_i of the iTED increases linearly with the addition of N and shows a linear behavior. From Fig. 8a, it is noticed that the change in heat transfer rates (Q_{h1}–Q_{h8}) at the inter-connector walls of each leg is minimal with the addition of N. However, the total Q_h increases with the addition of N. The P_0, Ohmic and Seebeck potentials increase significantly and illustrate more than two, three and threefold increases, respectively, at $N = 5$ compared to $N = 1$ values. On the other hand, both the η and the I decrease by nearly 33%, at $N = 5$ when compared to $N = 1$ values. Furthermore, a linear trend in $\Delta P/L$ with an addition of modules N is observed.

5. Conclusions

The performance of an integrated thermoelectric device (iTED) applied to waste-heat recovery has been investigated using three-dimensional fluid-thermo-electric coupled field numerical simulations. The influence of hot fluid temperatures T_{in}, thermoelectric elements sizes d and the number of modules N on iTED's performance have been studied for different fluid flow configurations Re.

An increment in either Re or T_{in} shows an enhancement in the device performance. The increase in Re or T_{in} produces larger temperature differentials (T_h–T_c) in thermoelectric materials and thus resulted in higher Seebeck voltages which in turn produced greater power output. Further, a linear behavior in produced electric current I, voltages V and efficiency η values and a non-linear trend in power output P_0 and heat input Q_h with T_{in} are observed.

An increase in d results in an increase in both thermo-electric resistances and Seebeck voltages and a decrease in Q_h values. For a given set of conditions, it is noticed that there exists an optimum d value where a maximum P_0 occurs. An exponentially increase trend in η and voltages and a linear decrease in I with an increase in d are observed. Further, the effect of d on the pressure drop $\Delta P/L$ is shown marginal.

As the number of modules N increases, R_i, Q_h, P_0 and the Ohmic and Seebeck voltages increase substantially; conversely, η and I decrease as a response to the increasing aforementioned values.

It is recommended to use fluid flow, heat transport and electrical coupling field simulations to capture the thermoelectric performance of state-of-the-art integrated thermoelectric devices.

References

[1] Rowe DM, editor. Thermoelectrics handbook macro to nano. Boca Raton: CRC Press, Taylor and Francis Group; 2006.
[2] Snyder GJ, Toberer ES. Complex thermoelectric materials. Nat Mater 2008;7:105–14.
[3] Minnich AJ, Dresselhaus MS, Ren ZF, Chen G. Bulk nanostructured thermoelectric materials: current research and future prospects. Energy Environ Sci 2009;2:466–79.
[4] Tritt TM. Thermoelectric phenomena, materials, and applications. Annu Rev Mater Res 2011;41:433–48.
[5] Caillat T, Fleurial JP, Snyder GJ, Zoltan A, Zoltan D, Borshchevsky A. Development of a high efficiency thermoelectric unicouple for power generation applications. In: Proceedings of the XVIII international conference on thermoelectrics, Baltimore, USA; 1999.
[6] El-Genk MS, Saber HH, Caillat T. Efficient segmented thermoelectric unicouples for space power applications. Energy Convers Manage 2003;44:1755–72.
[7] Punnachaiya S, Kovitcharoenkul P, Thong-aram D. Development of low grade waste heat thermoelectric power generator. Songklanakarin J Sci Technol 2010;32(3):307–13.
[8] Liang G, Zhou J, Huang X. Analytical model of parallel thermoelectric generator. Appl Energy 2011;88:5193–9.
[9] Crane D, Koripella C, Jovovic V. Validating steady-state and transient modeling tools for high-power-density thermoelectric generators. J Electron Mater 2012;41(6):1524–34.
[10] Hadjistassou C, Kyriakides E, Georgiou J. Designing high efficiency segmented thermoelectric generators. Energy Convers Manage 2013;66:165–72.
[11] Gou X, Xiao H, Yang S. Modeling, experimental study and optimization on low-temperature waste heat thermoelectric generator system. Appl Energy 2010;87:3131–6.
[12] Hsiao Y, Chang W, Chen S. A mathematic model of thermoelectric module with applications on waste heat recovery from automobile engine. Energy 2010;35:1447–54.
[13] Harris R, Hogan T, Schock HJ, Shih TI-P. Heat transfer and electric current flow in a thermoelectric couple. In: 44th Aerospace sciences meeting and exhibition, vol. 575. AIAA, Reno, Nevada; 2006.
[14] Ziolkowski P, Poinas P, Leszczynski J, Karpinski G, Muller E. Estimation of thermoelectric generator performance by finite element modeling. J Electron Mater 2010;39(9):1934–43.
[15] Hodes M. Optimal pellet geometries for thermoelectric power generation. IEEE Trans Comp Pack Technol 2010;33(2):307–18.
[16] Jan B, Han S, Kim J-Y. Optimal design for micro-thermoelectric generators using finite element analysis. Microelectron Eng 2011;88:775–8.
[17] Chen M, Rosendahl LA, Condra T. A three-dimensional numerical model of thermoelectric generators in fluid power systems. Int J Heat Mass Trans 2011;54:345–55.
[18] Wang XD, Huang YX, Cheng CH, Lin DTW, Kang CH. A three-dimensional numerical modeling of thermoelectric device with consideration of coupling of temperature field and electric potential field. Energy 2012;47:488–97.
[19] Reddy BVK, Barry M, Li J, Chyu MK. Mathematical modeling and numerical characterisation of composite thermoelectric devices. Int J Therm Sci 2013;67:53–63.

[20] Meng JH, Zhang XX, Wang XD. Dynamic response characteristics of thermoelectric generator predicted by a three-dimensional heat-electricity coupled model. J Power Sources 2014;245:262–9.
[21] Karri MA, Thacher EF, Helenbrook BT. Comparison of different modeling approaches for thermoelectric elements. Energy Convers Manage 2011;52(3):1596–611.
[22] Gould CA, Shammas NYA, Grainger S, Taylor I. A novel 3D TCAD simulation of a thermoelectric couple configured for thermoelectric power generation. In: International conference on renewable energies and power quality, Spain; 2011.
[23] Reddy BVK, Barry M, Li J, Chyu MK. Three-dimensional multiphysics coupled field analysis of an integrated thermoelectric device. Num Heat Trans Part A 2012;62:933–47.
[24] Reddy BVK, Barry M, Li J, Chyu MK. Thermoelectric performance of novel composite and integrated devices applied to waste heat recovery. ASME J Heat Trans 2013;135(3):031706 (1–11).
[25] Domenicali CA. Stationary temperature distribution in an electrically heated conductor. J Appl Phys 1954;25:1310–1.
[26] Patankar S. Numerical heat transfer and fluid flow. Taylor and Francis; 1980.